AGU ADVANCING EARTH AND SPACE SCIENCE

Geophysical Research Letters®

RESEARCH LETTER
10.1029/2021GL095746

The Fractal Nature of Clouds in Global Storm-Resolving Models

Hannah M. Christensen[1] and **Oliver G. A. Driver**[1]

[1]Department of Physics, University of Oxford, Oxford, UK

Key Points:

- Global storm-resolving models are able to reproduce the fractal nature of clouds
- The fractal dimension of clouds is used as a model validation tool to assess convective organization
- The fractal dimension is sensitive to boundary layer closure

Supporting Information:

Supporting Information may be found in the online version of this article.

Correspondence to:

H. M. Christensen,
hannah.christensen@physics.ox.ac.uk

Citation:

Christensen, H. M., & Driver, O. G. A. (2021). The fractal nature of clouds in global storm-resolving models. *Geophysical Research Letters*, *48*, e2021GL095746. https://doi.org/10.1029/2021GL095746

Received 17 AUG 2021
Accepted 17 NOV 2021

Author Contributions:

Conceptualization: Hannah M. Christensen
Formal analysis: Oliver G. A. Driver
Methodology: Hannah M. Christensen, Oliver G. A. Driver
Software: Oliver G. A. Driver
Supervision: Hannah M. Christensen
Visualization: Hannah M. Christensen, Oliver G. A. Driver
Writing – original draft: Hannah M. Christensen, Oliver G. A. Driver

Abstract Clouds in observations are fractals: they show self-similarity across scales ranging from 1 to 1,000 km. This includes individual storms and large-scale cloud structures typical of organized convection. It is not known whether global storm-resolving models reproduce the observed fractal scaling laws for clouds and organized convection. We compute the fractal dimension of clouds using Himawari satellite data and compare this to global storm-resolving model simulations completed as part of the DYAMOND intercomparison project. We find cloud fields in these simulations are indeed fractal, and reproduce the observed fractal dimension to within 10%. We find the fractal dimension is sensitive to the choice of boundary layer parametrization scheme used in each model simulation, and not to the convection parametrization as might have been expected.

Plain Language Summary Clouds are fractals: they are similar in their appearance whether we consider individual storms, or massive organized cloud systems spanning 1,000 km. In this paper, we demonstrate that state-of-the-art high-resolution atmospheric simulations are able to mimic this behavior. We compute the fractal dimension of clouds, which quantifies how smooth or crinkly clouds are. The fractal dimension of the simulated cloud fields is within 10% of that observed. We find the fractal dimension is sensitive to choices made when building the computer model used to produce the simulations. Unexpectedly, we find that the choices made when deciding how to represent turbulence close to the surface are important, as opposed to choices made in how to represent thunderstorms. The physics underpinning the merging of clouds into large organized systems is largely unknown. Our paper highlights the ability of simulations to capture this behavior. This means that high-resolution models can be used as digital laboratories to study the physics underpinning this important process.

1. Introduction

Numerical models are a useful tool to understand the climate system. Low-resolution climate models are routinely used for long simulations to address questions related to long-term climate change, the physics of low-frequency climate variability, and the likelihood of rare events. However, persistent biases remain in these models (e.g., Flato et al., 2013). Many biases and inconsistencies between models can be traced to the approximations used when developing model parametrization schemes (e.g., Zelinka et al., 2020).

Recent years have seen an increase in the production of global storm-resolving (also called convection-permitting) atmospheric simulations. Global storm-resolving models directly simulate important processes that must be parametrized in conventional climate models, most notably deep convective clouds (Palmer & Stevens, 2019). This substantially improves the fidelity of clouds and precipitation in those models (Stevens et al., 2020). The high fidelity of these models enables us to use them as a digital laboratory to explore fundamental unsolved questions in atmospheric physics, such as the physics of convective organisation (Wing, 2019).

Before using storm-resolving models in this way, we must quantify and understand the differences and similarities between the models and the real world. This reveals what questions can and cannot be addressed using those models. Certainly, global storm-resolving models appear realistic when compared to observations. An example of this is the visual similarity between images of simulated cloud condensate fields and satellite images of the Earth (Stevens et al., 2019). Assessing a model simulation using a visual comparison with observed fields as described here has been coined the "Palmer-Turing test" (Palmer, 2016) by analogy with the Turing test for Artificial Intelligence. While it can be difficult at first glance to distinguish between model and observed data, on closer inspection, the satellite image can often be identified.

It has long been known that clouds exhibit self-similarity across scales ranging from 1 to 1,000 km (Lovejoy, 1982)—that is, they are *fractals*. This behavior can provide insights into the physics underlying convective aggregation (Haerter, 2019) and precipitation processes (Peters & Neelin, 2006). In particular, scaling relationships imply emergent laws and universal behavior (Lovejoy & Schertzer, 2013). The fractal behavior of clouds has been used to assess the fidelity of large eddy simulations (Siebesma & Jonker, 2000). However, the approach has not been used to assess simulations with domain sizes large enough to simulate convective aggregation. In particular, it is not known whether convection in global storm-resolving models reproduces the observed behavior. However, in order to use such models to understand the physics of convective aggregation, we must be confident that they represent this process well.

In this paper, we take the Palmer-Turing test as a starting point to assess global storm-resolving models. However, we seek to go further and *quantify* the extent to which a simulated cloud field appears similar to that observed. We achieve this by computing the fractal dimension of clouds. We use this approach to assess the ensemble of global storm-resolving simulations produced for the DYAMOND project. In Section 2, we describe the model and observational datasets used in this paper. In Section 3, we describe how to identify comparable cloud objects in satellite and model data, and the definition of the fractal dimension. In Section 4, we compare the fractal dimensions computed for observed and simulated cloud fields. The DYAMOND models differ from each other in terms of resolution, parametrization schemes, and other modeling choices: we assess which of these choices impacts convective aggregation as measured by the fractal dimension. Finally we discuss the significance of our results and draw conclusions in Section 5.

2. Data

2.1. DYAMOND Global Storm-Resolving Models

We evaluate the global storm-resolving simulations produced for the DYAMOND summer ensemble (Stevens et al., 2019). Each model simulation was initialized at 00:00 UTC on 1 August 2016 and spans 40 days. The models were initialized using the ECMWF 9 km analysis. Daily observed sea-surface temperatures and sea ice concentrations were used as boundary conditions. Top of atmosphere outgoing longwave radiation (OLR) is available for each model simulation, regridded to a consistent 0.1° grid. We discard the first 10 days of each simulation as "spin-up" as suggested in Stevens et al. (2019).

The DYAMOND protocol was deliberately simple and unprescriptive, to encourage as many groups to participate as possible. The model simulations differ in their choice of vertical resolution, model top, cumulus parametrization scheme, and boundary layer scheme, among many other modeling choices (Stevens et al., 2019). The linear resolution (square root of the maximum grid box size) ranges from 2.5 to 7.8 km for the core ensemble. In addition to the core ensemble, we analyze six simulations from the "incidental ensemble"; these simulations differ from the core simulations in their horizontal resolution and choice of cumulus parametrization, allowing us to test the sensitivity of fractal dimension to these modeling choices. See Table S1 of the online supporting information for details of the simulations used in this paper.

2.2. Observed Cloud Fields

We compare the global storm-resolving simulations to satellite-derived cloud fields. The Japan Meteorological Agency Himawari 8 satellite was the most sophisticated geostationary satellite in orbit in 2016, and was used in Stevens et al. (2019) to validate the DYAMOND simulations: we also use Himawari 8 data for consistency with that paper. Himawari 8 has been operational since July 2015 (Bessho et al., 2016). The satellite is positioned at 140.7 E, with local solar noon at 02:41 UTC. The derived cloud top temperature and total cloud optical thickness products used in this analysis are provided on a 5 km grid, with 10 min resolution, in daytime regions only.

2.3. Region

We restrict our attention to an area below the footprint of the Himawari satellite. Throughout the analysis we will approximate pixels as squares. This limits the latitudinal extent of the domain we can consider. We use data between 25°N and 25°S, such that the maximum fractional distortion in the longitudinal arclength is $\cos(25°) = 0.91$. The longitudinal range is 80–200°E.

3. Methods

3.1. Defining Cloud Objects

We follow the methodology presented in Lovejoy (1982). We first compute a binary cloud field from the observed cloud top temperature data using a threshold of T_{CT}: any pixel with cloud top temperature below this threshold is defined as a cloudy pixel. We consider thresholds which select cold, deep clouds. Setting the threshold colder restricts the number of clouds analyzed, while choosing a warmer threshold makes it harder to compare satellite to model data. A warmer threshold also reduces the number of clouds, because cloud objects that intersect the edge of the domain are discarded.

To compute equivalent binary cloud fields for each simulation, we must map between cloud top temperature and OLR fields. This is carried out in a two-stage process. First, we map between the OLR and the effective radiating temperature of the cloud, T_{rad}. The relationship is not simply that of a black body flux, because of absorption of radiation by the atmosphere above cloud top. We therefore use the empirically measured relationship of Vaillant De Guélis et al. (2017),

$$F_{TOA} = a\,T_{\text{rad}} + b \tag{1}$$

where the OLR, F_{TOA}, is in Wm^{-2}, $a = 2.0\ \text{Wm}^{-2}\text{K}^{-1}$ and $b = -310\ \text{Wm}^{-2}$. This linear relationship between OLR and cloud radiating temperature was originally identified by Ramanathan (1977).

The effective radiating temperature of the cloud will reflect the temperature some depth below the cloud top. To convert between cloud radiating and cloud top temperature, we compare the satellite cloud top temperature field to the cloud radiating temperature derived from one of the DYAMOND simulations following Equation 1. We use the ICON 2.5 km simulated field for this mapping, regridded to the same 5 km grid as the satellite data. We use model data from 15 min after initialization to ensure a strong equivalence between the simulated and observed cloud fields. Despite the short lead time, there are likely to be cloudy pixels in the model simulation where no cloud was observed in satellite data, and vice versa. To ensure we only compare locations where there is a high, thick cloud in both model and satellite data, we only compare pixels for which the Himawari cloud optical thickness is at least 2.5 and the ICON column integrated ice and water content exceeds 0.005 and 0.0 kg m^{-2}, respectively. A total least squares fit on the retained pixels produced

$$T_{\text{rad}} = 0.86 T_{\text{CT}} + 36.1 \tag{2}$$

where the cloud top temperature, T_{CT}, and radiating temperature, T_{rad}, are in K.

3.2. Area-Perimeter Fractal Dimension

The fractal dimension of an object can be measured in several different ways depending on the nature of the object in question, including the similarity dimension (Strogatz, 2015) or box-counting dimension (Walsh & Watterson, 1993). For two-dimensional objects, the area-perimeter relation is a natural choice (Lovejoy, 1982). This relation predicts a fractal dimension of the perimeter through equation $P \propto A^{D/2}$. The fractal dimension, D, is a measure of the complexity, or "crinkliness," of the perimeter, since a smooth perimeter of given length encloses more area than a complex one. In Text S1 and Figure S1 of the Supporting Information, we test the area-perimeter approach to computing fractal dimension by applying it to the Koch snowflake.

We compute an instantaneous fractal dimension for each observed cloud top temperature and simulated OLR field. After applying the relevant threshold to generate a binary cloud field, the images are cleaned by removing holes in each cloud object. We discard any clouds with size smaller than 24 pixels as it was not possible to accurately estimate the cloud perimeter for objects of this size and smaller (see Text S1 and Figure S1). Note that this pixel threshold means that the lower resolution model fields have a physically larger minimum size of cloud than the satellite fields. We finally remove any clouds which overlap the edge of the field, as the perimeters of these clouds would be anomalously smooth. An example binary cloud field can be found in Figure S2.

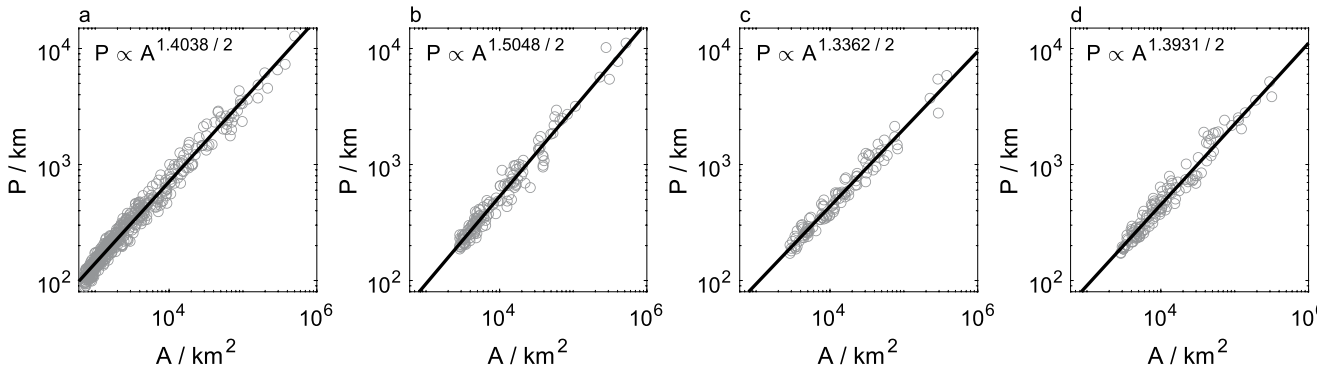

Figure 1. Cloud object perimeter as a function of area for (a) Himawari satellite data, and for (b) ICON 2.5 km, (c) IFS 4.8 km, and (d) NICAM 3.5 km simulations. The data correspond to fields at 0200 UTC on 11 August 2016, using $T_{CT} = 230$ K.

4. Results

4.1. Fractal Dimension of Cloud Objects

The area and perimeter of each cloud object in each binary field is measured. Figure 1a shows the measurements from 0200 UTC on 11 August 2016 of observed cloud objects identified from the satellite cloud top temperature field, using $T_{CT} = 230$ K. As demonstrated in Lovejoy (1982), the observed cloud objects are fractals, exhibiting the expected scaling behavior. Linear regression provides an estimate of the instantaneous fractal dimension, D, of 1.40, consistent with the value of 1.35 reported in Lovejoy (1982). Figures 1b and 1c show the equivalent area-perimeter measurements for simulated cloud fields from three of the models. We find that the cloud objects in the storm-resolving simulations also exhibit fractal behavior, showing a clean scaling relation similar to that observed in satellite data. The instantaneous fractal dimensions computed for each simulated field are close to the estimate from the satellite-derived image. The linear relationship shown for observed and simulated binary cloud fields supports monofractal behavior, as opposed to a multifractal scaling law.

The fractal dimension is computed separately for each day between 11 August and 9 September 2016 at 0200, 0300, and 0400 UTC. These times are close to local noon, for which satellite estimates of cloud top temperature are available. This analysis is performed for the satellite data and for each model simulation. The distribution of the computed fractal dimension D over this 30-day period is indicated in Figure 2, using $T_{CT} = 230$ K. All the global storm-resolving models simulate cloud fields that exhibit fractal behavior. The fractal dimension measured for the simulated cloud fields varies from model to model. For example, the ICON 2.5 and 5 km simulations have a notably higher fractal dimension than the other models (they have more crinkly clouds), while the IFS 4.8 km and NICAM 7 km simulations have a notably lower fractal dimension (they have smoother clouds). However, in general, the fractal dimension of the simulated cloud fields are all remarkably similar to that measured using satellite data, with the median dimension for all models falling within 10% of the observed value.

We repeated the fractal analysis for thresholds between 210 and 260 K to assess the sensitivity to the chosen threshold value. The median fractal dimension over the 30-day period is shown as a function of threshold in Figure 3. For the satellite data, colder thresholds result in a lower fractal dimension: colder, deeper clouds are smoother than warmer clouds. Most models reproduce this behavior. Notable exceptions are the UM and the MPAS 7.5 km simulation using a scale-aware convection parametrization.

Within the DYAMOND ensemble, the model set up differs substantially between simulations (Stevens et al., 2019). We consider whether any of the key choices made by the modeling groups contribute to the observed differences in simulated fractal dimension. The following discussion concerns the 230 K threshold, though equivalent conclusions were drawn at the other thresholds considered (not shown). Figure 4 shows the relationship between fractal dimension and the model resolution in both the horizontal and vertical. A small negative correlation (−0.29) is measured for horizontal resolution, while a small positive correlation (0.29) is measured for vertical resolution, though neither correlation is significant at the 95% level. The color of the data points in Figure 4 indicates the choice of (a) convection scheme and (b) boundary layer scheme. Interestingly, there is no systematic

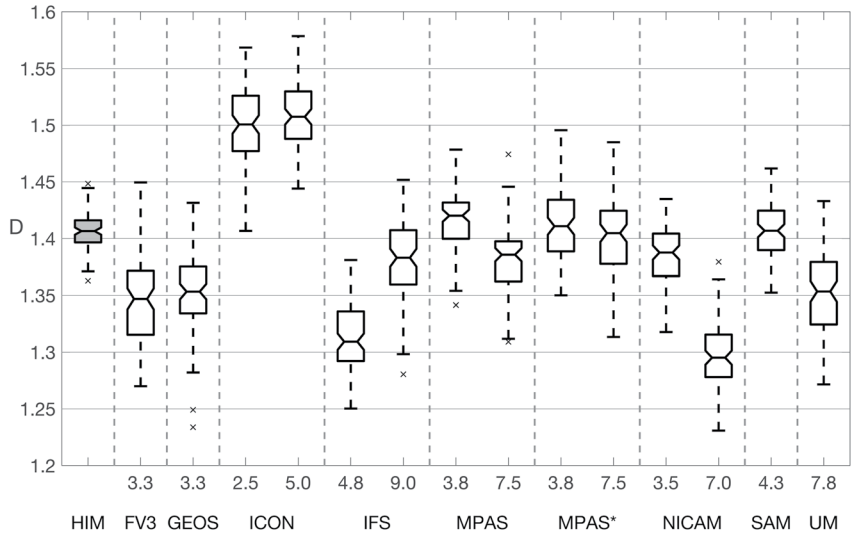

Figure 2. Box and whisker plot showing the distribution of fractal dimension, D, computed for Himawari satellite data (HIM: gray box plot) and each model simulation (white box plots), using $T_{CT} = 230$ K. The *x*-axis labels indicate the model and the resolution of each simulation in km. The MPAS* simulations use the convection parametrization, identical to that used in coarser simulations, while the simulations labeled MPAS use a scale-aware convection scheme. Each box top, waist, and bottom correspond to the 75th, 50th, and 25th percentiles, respectively. The whiskers indicate the range of the distribution. Crosses indicate outliers, defined as values that are more than 1.5 times the interquartile range away from the bottom or top of the box. The data correspond to 0200, 0300, and 0400 UTC for the last 30 days of the simulation (11 August–9 September 2016).

relationship between the choice of convection scheme and the simulated fractal dimension. However, sensitivity is observed in the choice of boundary layer scheme. Models which use a turbulent kinetic energy (TKE) scheme, in which closure involves solving a prognostic equation for TKE, systematically have a higher fractal dimension than models which use a diagnostic eddy-diffusivity scheme. We also considered the role of the height of the

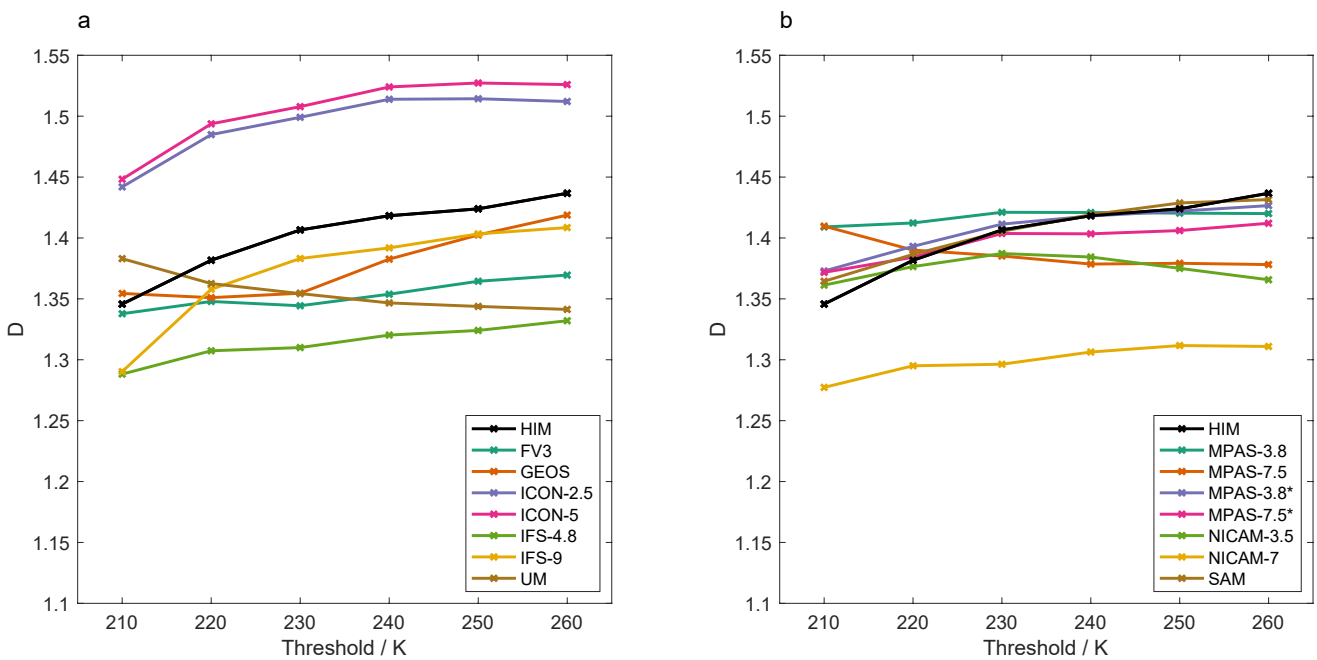

Figure 3. Median fractal dimension as a function of the cloud top temperature threshold used to define the binary cloud field, for satellite data and each model in turn. Legend labels as in Figure 2. The simulations (colors) are split into two subsets (a) and (b) for clarity. The data correspond to fields at 0200, 0300, and 0400 UTC for the last 30 days of the simulation (11 August–9 September 2016).

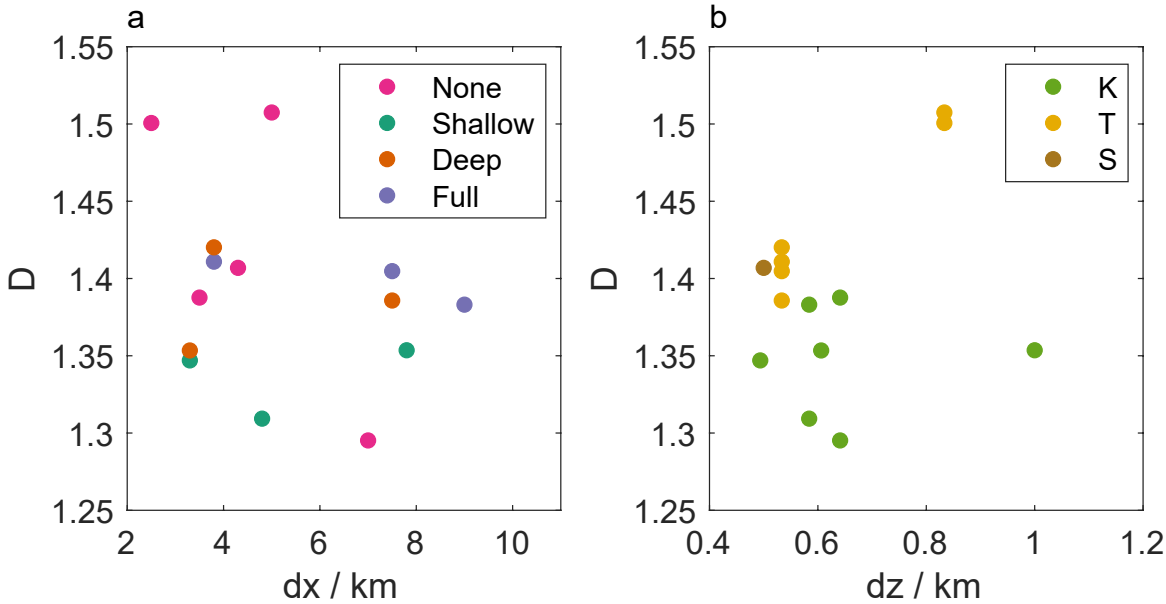

Figure 4. The fractal dimension, D, as a function of (a) the horizontal resolution and (b) the average vertical resolution, $dz = H_{top}/n_{lev}$, using $T_{CT} = 230$ (k) In (a), the marker colors indicate the cumulus parametrization scheme used: "none," "shallow," "deep," or "full," where the "deep" scheme has been re-tuned to account for the scales of motion being parametrized, whereas "full" is the un-tuned version also used at coarser resolutions. In (b) the marker colors indicate the boundary layer scheme used: "T," a TKE-type scheme, involving an additional prognostic equation; "K," a diagnostic eddy-diffusivity scheme; "S," a three-dimensional Smagorinsky-type scheme. The data correspond to 0200, 0300, and 0400 UTC for the last 30 days of the simulation (11 August–9 September 2016).

model top, the height of the sponge layer, and the number of vertical levels: none of these showed a significant impact on the simulated fractal dimension.

4.2. Distribution of Cloud Areas

We finally measure the distribution of cloud object areas. This complementary diagnostic also provides an independent assessment of whether the OLR and cloud top temperature thresholds are consistent with each other. Figure 5 shows the number of cloud objects, N, as a function of cloud object area, A, for the satellite and model data sets using a threshold of 230 K. The number of cloud objects as a function of size also follows a scaling law, $N = kA^{-\alpha}$, such that the data show linear relationships in log-log space (Figure 5). On average across the

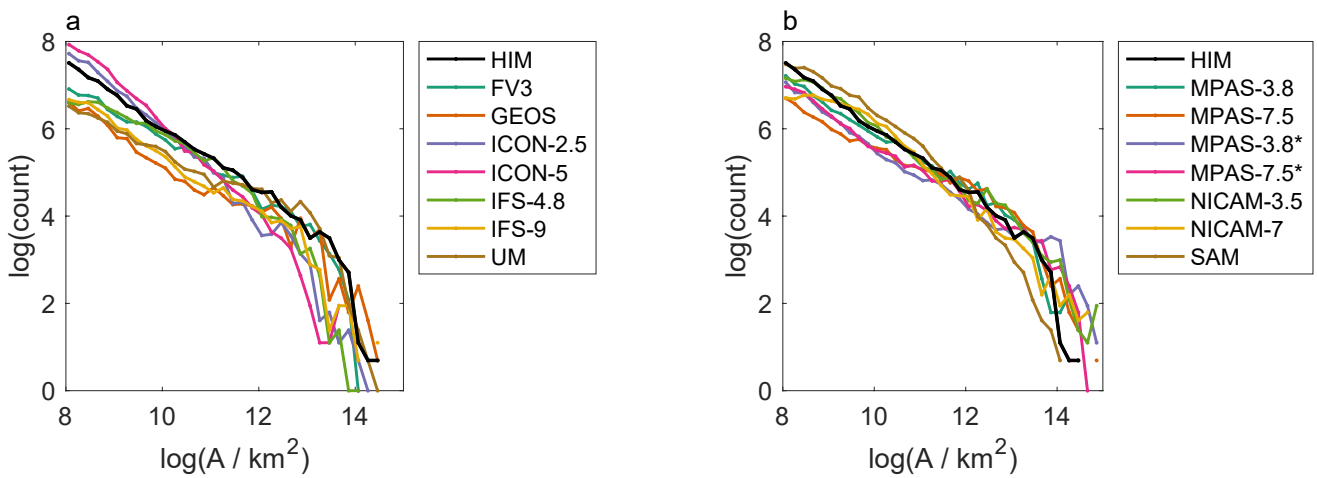

Figure 5. Number of cloud objects as a function of cloud object area, A, compared to Himawari satellite data (black). The simulations (colors) are split into two subsets (a) and (b) for clarity. The data correspond to 0200, 0300, and 0400 UTC for the last 30 days of the simulation (11 August–9 September 2016).

models, the simulated distributions match the observed distribution, suggesting the thresholds in OLR and cloud top temperature are indeed consistent. However, there are substantial differences between simulations produced using different models. When the same model is used but the resolution is varied, the resolution tends to have a large impact on the simulated distribution, except for the MPAS* simulations. This pair of simulations includes the same, un-tuned version of the convection scheme that is used at coarser resolutions. This indicates the MPAS model using the full convection scheme (MPAS*) has converged in some sense, while the model using the scale-aware convection scheme has not. For a description of the two MPAS convection schemes, see Judt and Rios-Berrios (2021).

The fractal dimension and the scaling properties of cloud object areas are related: the correlation coefficient between D and α was 0.81 (p value of 0.0002). Here, α was estimated from a linear fit to Figure 5 using cloud objects for which $\log(A) < 12$.

5. Discussion and Conclusions

We describe a novel methodology for examining the fidelity of cloud fields in high-resolution model simulations. We define a binary cloud field using a threshold in OLR or cloud top temperature, before examining the fractal nature of the resultant cloud objects. We demonstrate that global storm-resolving simulations produced for the DYAMOND project (Stevens et al., 2019) are able to reproduce the observed fractal nature of clouds. In other words, the area and perimeter of cloud objects are related by the scaling law $P \propto A^{D/2}$ where D is the fractal dimension. The fractal nature of clouds is an emergent property of models. It gives us confidence that these global storm-resolving models are representing the key aspects of the physics of clouds, convection, and convective organization and aggregation.

In addition to reproducing the fractal nature of clouds, the fractal dimension of clouds in these simulations is close (within 10%) to that of cloud fields observed by the Himawari 8 geostationary satellite. To explain differences in the fractal dimension between models, we considered the modeling choices made when producing each of the DYAMOND simulations. The different simulations vary substantially in their model setups, including the model horizontal and vertical resolutions, the type of boundary layer scheme used, and whether any part of the model's convection parametrization scheme is activated. Of these choices, the only significant predictor of fractal dimension was the choice of boundary layer scheme. Models which included a prognostic equation for TKE had a higher fractal dimension than those which use an eddy-diffusivity scheme. This highlights the importance of the boundary layer scheme for convective organisation *as opposed to the convection scheme*. The comparative role of these two parametrization schemes in organizing convection is poorly known, though some single-model studies have highlighted the importance of the choice of boundary layer scheme for phenomena such as the Madden–Julian Oscillation (MJO) (Holloway et al., 2013), consistent with the Convective-Dynamic-Moisture trio-interaction theory of the MJO (Zhang et al., 2020). More generally, it is known that the different approximations used in boundary layer parametrizations can significantly impact the climate in models, including the model's climate sensitivity (Davy & Esau, 2014, 2016; Garratt, 1993).

While the binary cloud fields considered in this study exhibit monofractal behavior, characterized by a single fractal dimension, the full cloud field (as represented continuously by its OLR) is *multifractal*, and is characterized by an infinite hierarchy of dimensions (e.g., Lovejoy & Schertzer, 1990). The dependency of the measured monofractal dimension on the threshold used to create the binary fields hints at this underlying multifractal behavior. The fact that some models were not able to reproduce the dependency of dimension on threshold indicates that multifractal analysis could be a sharper tool with which to assess global storm-resolving models. This will be the topic of future work.

One motivations of this study was to quantify the "Palmer-Turing test" (Palmer, 2016). This test suggests that we can assess the fidelity of climate models by visually comparing instantaneous maps of model output to satellite observations. If we cannot tell which image is simulated and which is observed, then the model has passed the Palmer-Turing test. We suggested that the fractal dimension of cloud objects would be a useful tool to quantify the visual similarities and differences noted when performing the Palmer-Turing test, which are otherwise difficult to enunciate. It is instructive to return at this point to the images of the simulated condensate fields from the DYAMOND simulations (Stevens et al., 2019, Figure 2). The model whose instantaneous fractal dimension

is closest to Himawari at 0400 UTC on 4 August 2016 is MPAS (both Himawari and MPAS have $D = 1.43$ for $T_{CT} = 230$ K), followed by SAM and the IFS 9 km simulation. We note that these three models are visually different to each other. The fractal dimension alone does not fully characterize the image. In particular, low cloud and the distribution of cloud object sizes also influence our impression. Nevertheless, the fractal dimension is a useful additional tool for quantifying the ability of models to simulate deep convection and convective organisation.

Data Availability Statement

The processed cloud data produced in this study can be downloaded from https://doi.org/10.5281/zenodo.5596645 (https://doi.org/10.5281/zenodo.5596645) under a GNU general public license v2.0 (Christensen and Driver, 2021). DYAMOND data are archived by the German Climate Computing Center (DKRZ) and made available through the ESiWACE project (https://www.esiwace.eu/services/dyamond). The cloud properties derived from Himawari-8 that were used in this paper were supplied by the P-Tree System, Japan Aerospace Exploration Agency (JAXA: https://www.eorc.jaxa.jp/ptree/userguide.html).

Acknowledgments
The authors thank Simon Proud for assistance with the Himawari 8 data, and Daniel Klocke, Florian Ziemen, and Julia Duras for assistance with the DYAMOND data. Hannah M. Christensen was funded by Natural Environment Research Council grant number NE/P018238/1. DYAMOND data management was provided by the German Climate Computing Center (DKRZ) and supported through the projects ESiWACE and ESiWACE2, which were funded by the European Union's Horizon 2020 research and innovation program under grant agreements No 675191 and 823988. This work used resources of the DKRZ granted by its Scientific Steering Committee (WLA) under project IDs bk1040 and bb1153.

References

Bessho, K., Date, K., Hayashi, M., Ikeda, A., Imai, T., Inoue, H., et al. (2016). An introduction to Himawari-8/9 — Japan's new-generation geostationary meteorological satellites. *Journal of the Meteorological Society of Japan*, *94*(2), 151–183. https://doi.org/10.2151/jmsj.2016-009

Christensen, H. M., & Driver, O. G. A. (2021). *Fractal Analysis of Clouds in DYAMOND Summer Simulations* (revised) [Data set]. Zenodo. https://doi.org/10.5281/zenodo.5596645

Davy, R., & Esau, I. (2014). Global climate models' bias in surface temperature trends and variability. *Environmental Research Letters*, *9*(11), 114024. https://doi.org/10.1088/1748-9326/9/11/114024

Davy, R., & Esau, I. (2016). Differences in the efficacy of climate forcings explained by variations in atmospheric boundary layer depth. *Nature Communications*, *7*(1), 1–8. https://doi.org/10.1038/ncomms11690

Flato, G., Marotzke, J., Abiodun, B., Braconnot, P., Chou, S. C., Collins, W., & Rummukainen, M. (2013). Evaluation of climate models, et al. (Eds.). In *Climate change 2013: The physical science basis. Contribution of working group I to the fifth assessment report of the intergovernmental panel on climate change*. Cambridge University Press.

Garratt, J. R. (1993). Sensitivity of climate simulations to land-surface and atmospheric boundary-layer treatments — A review. *Journal of Climate*, *6*, 419–448. https://doi.org/10.1175/1520-0442(1993)006<0419:socstl>2.0.co;2

Haerter, J. O. (2019). Convective self-aggregation as a cold pool-driven critical phenomenon. *Geophysical Research Letters*, *46*(7), 4017–4028. https://doi.org/10.1029/2018GL081817

Holloway, C. E., Woolnough, S. J., & Lister, G. M. S. (2013). The effects of explicit versus parameterized convection on the MJO in a large-domain high-resolution tropical case study. Part I: Characterization of large-scale organization and propagation. *Journal of the Atmospheric Sciences*, *70*(5), 1342–1369. https://doi.org/10.1175/JAS-D-12-0227.1

Judt, F., & Rios-Berrios, R. (2021). Resolved convection improves the representation of equatorial waves and tropical rainfall variability in a global nonhydrostatic model. *Geophysical Research Letters*, *48*(14), 1–10. https://doi.org/10.1029/2021GL093265

Lovejoy, S. (1982). Area-perimeter relation for rain and cloud areas. *Science*, *216*(4542), 185–187. https://doi.org/10.1126/science.216.4542.185

Lovejoy, S., & Schertzer, D. (1990). Multifractals, universality classes and satellite and radar measurements of cloud and rain fields. *Journal of Geophysical Research*, *95*(D3), 2021–2034. https://doi.org/10.1029/JD095iD03p02021

Lovejoy, S., & Schertzer, D. (2013). *The weather and climate: Emergent laws and multifractal cascades*. Cambridge University Press.

Palmer, T. N. (2016). A personal perspective on modelling the climate system. *Proceedings of the Royal Society A: Mathematical, Physical & Engineering Sciences*, *472*(2188), 472. https://doi.org/10.1098/rspa.2015.0772

Palmer, T. N., & Stevens, B. (2019). The scientific challenge of understanding and estimating climate change. *Proceedings of the National Academy of Sciences of the United States of America*, *116*(49), 34390–24395. https://doi.org/10.1073/pnas.1906691116

Peters, O., & Neelin, J. D. (2006). Critical phenomena in atmospheric precipitation. *Nature Physics*, *2*(6), 393–396. https://doi.org/10.1038/nphys314

Ramanathan, V. (1977). Interactions between Ice-Albedo, Lapse- Rate and cloud-top feedbacks: An analysis of the nonlinear response of a GCM climate model. *Journal of the Atmospheric Sciences*, *34*, 1885–1897. https://doi.org/10.1175/1520-0469(1977)034<1885:ibialr>2.0.co;2

Siebesma, A. P., & Jonker, H. J. J. (2000). Anomalous scaling of cumulus cloud boundaries. *Physical Review Letters*, *85*, 214–217. https://doi.org/10.1103/physrevlett.85.214

Stevens, B., Acquistapace, C., Hansen, A., Heinze, R., Klinger, C., Klocke, D., et al. (2020). The added value of large-eddy and storm-resolving models for simulating clouds and precipitation. *Journal of the Meteorological Society of Japan*, *98*(2), 395–435. https://doi.org/10.2151/jmsj.2020-021

Stevens, B., Satoh, M., Auger, L., Biercamp, J., Bretherton, C. S., Chen, X., & Zhou, L. (2019). Open Access DYAMOND: The DYnamics of the Atmospheric general circulation Modeled On Non-hydrostatic Domains. *Progress in Earth and Planetary Science*, *6*(1), 1–17.

Strogatz, S. H. (2015). *Nonlinear dynamics and chaos: With applications to physics, biology, chemistry, and engineering* (2nd ed.). Westview Press.

Vaillant De Guélis, T., Chepfer, H., Noel, V., Guzman, R., Dubuisson, P., Winker, D. M., & Kato, S. (2017). The link between outgoing longwave radiation and the altitude at which a spaceborne lidar beam is fully attenuated. *Atmospheric Measurement Techniques*, *10*(12), 4659–4685. https://doi.org/10.5194/amt-10-4659-2017

Walsh, J. J., & Watterson, J. (1993). Fractal analysis of fracture patterns using the standard box-counting technique: Valid and invalid methodologies. *Journal of Structural Geology*, *15*(12), 1509–1512. https://doi.org/10.1016/0191-8141(93)90010-8

Wing, A. A. (2019). Self-aggregation of deep convection and its implications for climate. *Current Climate Change Reports*, *5*(1), 1–11. https://doi.org/10.1007/s40641-019-00120-3

Zelinka, M. D., Myers, T. A., McCoy, D. T., Po-Chedley, S., Caldwell, P. M., Ceppi, P., et al. (2020). Causes of higher climate sensitivity in CMIP6 models. *Geophysical Research Letters*, *47*(1), 1–12. https://doi.org/10.1029/2019GL085782

Zhang, C., Adames, Á. F., Khouider, B., Wang, B., & Yang, D. (2020). Four theories of the Madden-Julian oscillation. *Reviews of Geophysics*, *58*, e2019RG000685. https://doi.org/10.1029/2019rg000685